Dynamics of rotary drilling with non-uniformly distributed blades

Accepted Manuscript

Dynamics of rotary drilling with non-uniformly distributed blades

Yao Yan, Marian Wiercigroch

Please cite this article as: Yao Yan, Marian Wiercigroch, Dynamics of rotary drilling with non-uniformly distributed blades, *International Journal of Mechanical Sciences* (2019), doi: https://doi.org/10.1016/j.ijmecsci.2019.05.016
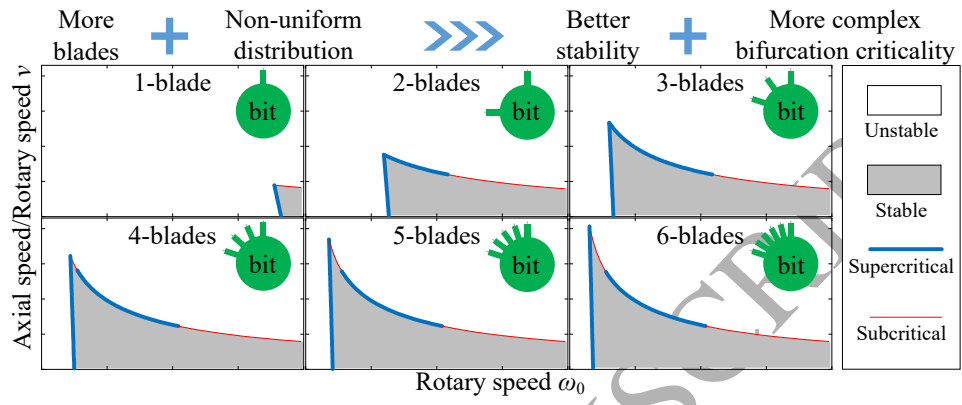
Highlights

- Dynamics of drilling with non-uniform blades distribution is studied.

- More blades and non-uniform distribution benefit drilling stability.

- Improvement of stability is accompanied with more complex bifurcation scenarios.

- Slow rotary speed yields more complexity in nonlinear drilling chatter.

Graphical Abstract

Dynamics of rotary drilling with non-uniformly distributed blades

Yao Yan[a,b,*], Marian Wiercigroch[c]

[a]*School of Aeronautics and Astronautics, University of Electronic Science and Technology of China, Chengdu 611731, China*
[b]*Aircraft swarm intelligent sensing and cooperative control Key Laboratory of Sichuan Province, University of Electronic Science and Technology of China, Chengdu 611731, China*
[c]*Centre for Applied Dynamics Research, School of Engineering, Fraser Noble Building, King's College, University of Aberdeen, Aberdeen, AB24 3UE Scotland, UK*

Abstract

This paper investigates the linear stability and nonlinear dynamics of drilling with non-uniformly distributed blades in the drill-bit. The analysis is based on a lumped parameter model considering both axial and torsional drill-string deformation, with both regenerative cutting and frictional effects in bit-rock interaction considered as sources of drilling instability. Given the flexibility of angles' selection introduced by the non-uniform blade distribution, eigenvalue analysis reveals that letting one angle occupy the majority of the angles summation and introducing an extra blade can enlarge the stable region for stationary drilling. Then perturbation analysis finds both subcritical and supercritical types of instability on the stability boundaries, where the subcritical Hopf bifurcation introduces large-amplitude oscillations to deteriorate the global drilling stability in the regions close to the up-left and up-right areas of the stable regions. Moreover, numerical bifurcation analysis of drilling with 3 non-uniformly distributed blades discovers various complex nonlinear dynamics including bit-bounce, stick-slip motion, loss of contact.

Keywords: drill-string vibration, non-uniform distribution of blades, state-dependent delay, bit-bounce, stick-slip

[*]Corresponding author
Email address: y.yan@uestc.edu.cn (Yao Yan)

1. Introduction

A typical drilling system uses a rotary table to drive a series of hollow drill-strings ended with a section called bottom-hole assembly (BHA), which consists of thick drill-collars, stabilizers and drill-bit exerting Weight-On-Bit (WOB) and Torque-On-Bit (TOB) for down-hole drilling [1]. During the progression of drill-bit, unwanted vibratory drill-strings deformation often arise to cause premature component failures, excessive bit and stabilizer wear, deterioration of well trajectory and low penetration rate, which rises roughly 2%-10% well costs in the manner of poor quality wellbore, increased service cost, etc [2, 3]. Thus the drill-string vibration should be avoided while pursuiting higher drilling efficiency, where sophisticated modelling of slender drill-strings deformation and complex bit-rock interaction are expected for the analysis of uncoupled or coupled types of axial, torsional and lateral drill-string vibration.

Models of the slender drill-strings deformation has been classified into four categories: lumped parameter, distributed parameter, neutral-type time-delay and coupled PDE-ODE models [4]. Both of the distributed parameter and coupled PDE-ODE models employ partial differential equations (PDEs) to represent the drill-sting deformation, which are relative accurate but infinite many dimensions of the drill-string crucially complicate the analysis of drilling dynamics, especially when a complex bit-rock interactive model is used [5]. Alternatively, delayed differential equations (DDEs) can be used as well to represent wave propagation in the slender drill-string [6], which is relative simpler but still has infinite dimensions due to the introduction of time delays. Among the four kinds of models, the lumped parameter one is the simplest, which uses ordinary differential equations (ODEs) involving one or multiple degrees-of-freedom (DOF) for various drilling dynamics of interest [7].

Beside the drill-string deformations, the instability sources should be modelled accurately as well for different drilling vibrations [8]. For example, the axial vibration is attributed to regenerative effect during blade cuts into rocks,

4

30 which causes bit-bounce and damages bit cutter and bearings [9]. Meanwhile, there also exists velocity-dependent frictional force in the bit-rock interaction as the instability source of torsional drill-string vibration, inducing stick-slip vibration and fatiguing drill collars connections [10]. The lateral drill-string vibration, which occurs as forward and backward whirling oscillations, is mainly

35 caused by dill-pipe eccentricities and asymmetries, resulting in large-amplitude response, impact with borehole wall and high rates of component failures [11].

In addition to individual types of drilling instability, the effect of mode-coupling is also very crucial. Richard *et al.* [12] found the coupling of axial and torsional drill-string movements can be the cause of stick-slip vibration beside

40 the velocity-dependent friction. His model was then updated by Besselink *et al.* [13] to involve finite axial stiffness and viscous damping in the drill-string, which was used to study the stick-slip instability caused by axial bit-rock interactive force. Thereafter, the axial damping was added by Nandakumar and Wiercigroch [14] for the analysis of drilling stability and prediction of bit-bounce and

45 stick-slip oscillations. This linear analysis was followed by studying criticality of bifurcation in the drilling model, where Gupta and Wahi [15] observed both subcritical and supercritical Hopf bifurcations on linear stability boundaries.

Recently, Wiercigroch *et al.* [16] further developed the model proposed in [14] by considering non-uniformly distributed blades in the drill-bit, which per-

50 turbs the regenerative effect and can potentially improve the drilling stability. The effect of non-uniform distribution of blades is somewhat similar to milling operations using variable pitch or variable helix tools, which can destroy the periodicity of the regenerative effect between successive passes of adjacent blades (teeth) [17]. However, there is no investigation of the stability and dynamics

55 of non-uniform drilling up to now, so its advantages are still theoretically unknown. To reveal its mechanism, one should study the relationship between the angles distribution and rock surface regeneration, which acts as the instability source of drill-string's axial deformation.

Investigation of the regenerative phenomenon is originated from the works

60 performed by Arnold [18] and Tobias [19], who disclosed that regeneration of

5

workpiece surface is responsible for turning chatter. For any point in the workpiece surface, one pass of a cutting tool leaves a mark recording the tool displacement, which perturbs the tool motion after one workpiece revolution. This regenerative effect gradually induces periodic vibration when energy dissipation of the turning system is insufficient, leaving chatter marks on the whole workpiece surface [20]. Similar phenomena can also been found in other cutting operations, such as milling, grinding and drilling processes [21, 22, 23]. More specifically for the borehole drilling, its drill-bit normally has numerous blades dynamically interacting with each others via regenerative effect in rock surface. As there is no general guidelines for the organization of the blades up to now, a thorough discussion of the effect of blades distribution is very critical for the improvement of drilling stability and efficiency.

The effect of non-uniform blades distribution in the drill-bit is studied as follows. A lumped parameter model involving both axial and torsional drill-string deformations is proposed in Section 2, which consists of state-dependent delays and non-smoothness in the bit-rock interaction. Then Section 3 studies the influence of blades number and their distributions on the stability boundaries, which confirms the advantages of using more blades and non-uniform distribution in the drill-bit. After that, both local and global bifurcation analyses are performed in Section 4, discovering multi-stability, bit-bounce, stick-slip and other complex drilling dynamics. Finally, conclusions are drawn in Section 5.

2. Description of drilling process and governing mathematical model

To focus on the effect of bit-rock interaction on the axial-torsional drill-string vibration, this section employs the simple lumped parameter model shown in Fig. 1, without considering lateral whirling of the drill-string. Correspondingly, a dynamic model with 2 DOF, which involves regenerative and frictional effects [24] in the bit-rock interaction, is proposed and nondimensionalized to discuss the vertical translation and rotation of the drill-bit.
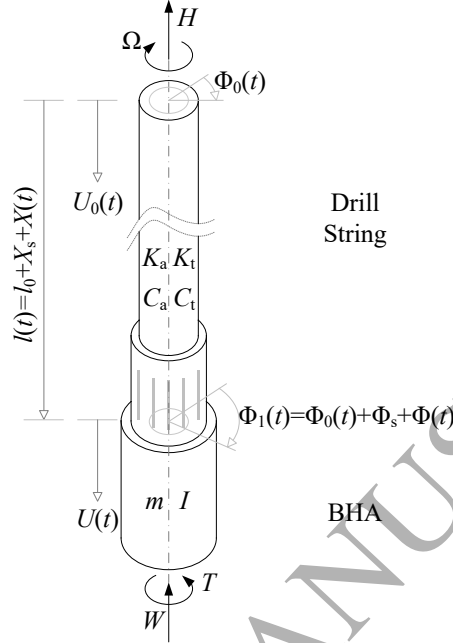
6

Figure 1: Schematic of the lumped parameter model, where the inertial properties (m and I) are lumped at the BHA and the slender drill-string has only damping (C_a and C_t) and elastic (K_a and K_t) properties. The top of the string is driven with constant angular speed (Ω) and hook load (H), and the BHA suffers reactive force (W) and torque (T) from rock.

2.1. Modelling

As seen in Fig. 1, the slender drill-string has equivalent axial and torsional stiffness, K_a [N m^{-1}] and K_t [N m rad^{-1}], and damping, C_a [N s m^{-1}] and C_t [N m s rad^{-1}], respectively [14]. At the top of the drill-string, draw-works and electric motors are used to control vertical and rotary movements of the BHA via the slender string, applying a constant hook load H [N], an angular speed Ω [rad s^{-1}] and a linear downward speed V [m s^{-1}] on the drill-string.

With respect to the driven system, vertical and angular positions of the string top can be written as

$$U_0(t) = Vt \quad \text{and} \quad \Phi_0(t) = \Omega t. \tag{1}$$

Given the length and deformation of the drill-string, the vertical and angular

7

positions of the BHA are denoted as

$$U(t) = U_0(t) + l_0 + X_{\mathrm{s}} + X(t) \quad \text{and} \quad \Phi_1(t) = \Phi_0(t) + \Phi_{\mathrm{s}} + \phi(t), \qquad (2)$$

where $U(t)$ [m] and $\Phi_1(t)$ [rad] represent the vertical and torsional positions of the first blade on the drill-bit, and l_0, X_{s} and $X(t)$ are the free length, vertical static and dynamic deformations of the string, respectively. Similarly, the static and dynamic torsional deformations of the string are denoted as Φ_{s} and

100 $\phi(t)$ respectively in Eq. (2). When the progression of the drill-bit is stabilised at the constant vertical and rotary speeds, V and Ω, without any dynamics responses, the drill-string has only the static deformations, X_{s} and Φ_{s}, with $X(t) = \phi(t) \equiv 0$.

When the rotational drill-bit moves against rocks, reactive forces are generated and exerted on the BHA to excite its dynamics governed by

$$m\ddot{U}(t) + C_{\mathrm{a}}\dot{U}(t) + K_{\mathrm{a}}(U(t) - U_0(t) - l_0) = -W,$$
$$I\ddot{\Phi}_1(t) + C_{\mathrm{t}}\dot{\Phi}_1(t) + K_{\mathrm{t}}(\Phi_1(t) - \Phi_0(t)) = -T, \qquad (3)$$

or

$$m\ddot{X}(t) + C_{\mathrm{a}}(V + \dot{X}(t)) + K_{\mathrm{a}}(X_{\mathrm{s}} + X(t)) = -\sum_{i=1}^{n} W_i,$$
$$I\ddot{\phi}(t) + C_{\mathrm{t}}(\Omega + \dot{\phi}(t)) + K_{\mathrm{t}}(\Phi_{\mathrm{s}} + \phi(t)) = -\sum_{i=1}^{n} T_i, \qquad (4)$$

where W and T are the overall reactive vertical force and torque exerted by

105 rocks on the drill-bit, and W_i and T_i $(i = 1, 2, \cdots, n)$ are individual ones on the ith blade. Here, the dots over the variables in Eqs (3) and (4) represent the derivatives with respective to time, t.

For each blade engaged with rocks, its cutting face cuts and its wearflat rubs the rock to respectively generate cutting and frictional forces [12]. Thus both the reactive force and torque on the ith $(i = 1, 2, \cdots, n)$ blade have cutting and frictional components:

$$W_i = W_{\mathrm{c},i} + W_{\mathrm{f},i} \quad \text{and} \quad T_i = T_{\mathrm{c},i} + T_{\mathrm{f},i}. \qquad (5)$$

8

According to the experimental results reported by Detournay *et al.* [25], the cutting force and torque on each blade are given by

$$W_{c,i} = \xi \epsilon a d_i(t) H(d_i) H(\dot{\Phi}_i) \quad \text{and} \quad T_{c,i} = \frac{a^2 \epsilon d_i(t)}{2} H(d_i) H(\dot{\Phi}_i), \qquad (6)$$

where a, $d_i(t)$, ϵ and ξ are bit radius, instantaneous cutting depth of the ith blade, intrinsic specific energy of the rock and inclination of the cutting forces on the cutting face, respectively. Besides, the overall frictional components of the WOB and TOB are

$$W_{f,i} = \sigma a l_i H(d_i) H(\dot{U}) \quad \text{and} \quad T_{f,i} = \frac{\mu \gamma a W_{f,i}}{2} \mathrm{sgn}(\dot{\Phi}_i), \qquad (7)$$

where γ is related to the orientation of the cutter, σ is the maximum contact pressure at bit-rock interface, and $l_i = \frac{l}{n}$ is the mean wear-flat length of every

110 cutters. In Eqs (6) and (7), $H(\bullet)$ and $\mathrm{sgn}(\bullet)$ are Heaviside and sign functions representing the non-smoothness in the bit-rock interaction [26]. Those effects would not show up until the drill-string response extensively deviates from the its stationary deformation, so that the non-smoothness can be omitted first in the following static and linear analysis but will be considered in the investigation

115 of nonlinear drilling dynamics.

From Eqs (5), (6) and (7), W and T in the governing equations of the drilling dynamics can be rewritten as

$$
\begin{aligned}
W &= \xi \epsilon a \sum_{i=1}^{n} d_i H(d_i) H(\dot{\Phi}_i) + \sigma a l \frac{\sum_{i=1}^{n} H(d_i) H(\dot{U})}{n}, \\
&= \xi \epsilon a H(\Omega + \dot{\phi}) \sum_{i=1}^{n} d_i H(d_i) + \sigma a l H(V + \dot{X}) \frac{\sum_{i=1}^{n} H(d_i)}{n} \\
T &= \frac{a^2 \epsilon}{2} \sum_{i=1}^{n} d_i H(d_i) H(\dot{\Phi}_i) + \frac{\mu \gamma a^2 \sigma}{2} \frac{\sum_{i=1}^{n} H(d_i) H(\dot{U})}{n} \mathrm{sgn}(\dot{U}) \\
&= \frac{a^2 \epsilon}{2} H(\Omega + \dot{\phi}) \sum_{i=1}^{n} d_i H(d_i) + \frac{\mu \gamma a^2 \sigma l}{2} H(V + \dot{X}) \mathrm{sgn}(V + \dot{X}) \frac{\sum_{i=1}^{n} H(d_i)}{n} m,
\end{aligned}
$$
$$(8)$$

where the instantaneous cutting depth of the ith blade, $d_i(t)$, can be determined based on regenerative theory. As seen in Fig. 2, $d_i(t)$ is the difference of current
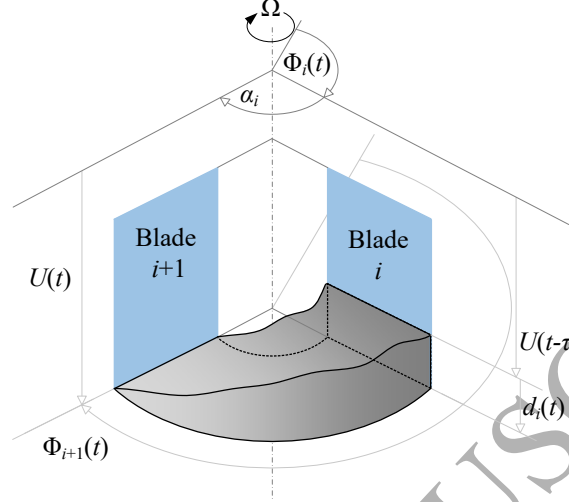
9

Figure 2: Regenerative effect in the interaction between drag bit and rock, where the ith blade cut into the rock surface generated by the pass of the $(i+1)$th blade. Thus the instantaneous cutting depth of the ith blade is the difference of the two successive blade passes.

axial displacement of the ith blade, $U(t)$, and previous displacement of the $(i+1)$th blade, $U(t - t_i)$:

$$d_i(t) = U(t) - U(t - t_i) = Vt_i + X(t) - X(t - t_i), \quad i = 1, 2, \cdots, n, \qquad (9)$$

where t_i is the time difference for the two blades successively passing the same point. Given the distribution of the blades and the torsional vibration of the drill-string, t_i is implicitly governed by

$$\Phi_i(t) - \Phi_{i+1}(t - t_i) = \Omega t_i + \phi(t) - \phi(t - t_i) = \alpha_i, \quad i = 1, 2, \cdots, n, \qquad (10)$$

where $\Phi_{n+1} = \Phi_1$ also indicates the 1st blade.

2.2. Model nondimensionalization

To simplify the following analyses, an effective method is to nondimensionalize the governing equation of the drilling process. By letting $L = \frac{2K_t}{\epsilon a^2}$ and introducing the following dimensionless variables

$$x = \frac{X}{L}, \quad \delta_i = \frac{d_i}{L}, \quad \tau = \sqrt{\frac{K_t}{I}}t, \quad \tau_i = \sqrt{\frac{K_t}{I}}t_i, \qquad (11)$$

10

and parameters

$$\delta_0 = \frac{V}{L}\frac{2\pi}{\Omega}, \quad \omega_0 = \Omega\sqrt{\frac{I}{K_\mathrm{t}}}, \quad v_0 = \frac{V}{L}\sqrt{\frac{I}{K_\mathrm{t}}} = \frac{\delta_0\omega_0}{2\pi},$$

$$\psi = \frac{\xi a\epsilon I}{mK_\mathrm{t}}, \quad \zeta = \frac{C_a}{2\sqrt{K_a m}}, \quad \beta = \sqrt{\frac{K_\mathrm{a}I}{K_\mathrm{t}m}}, \quad \kappa = \frac{C_\mathrm{t}}{2\sqrt{K_\mathrm{t}I}}, \tag{12}$$

$$x_\mathrm{s} = \frac{X_\mathrm{S}}{L}, \quad f_x = \frac{I\sigma al}{mK_t Ln}, \quad f_\phi = \frac{\mu\gamma\sigma a^2 l}{2K_t n},$$

one can change Eq. (4) into its dimensionless form as follows

$$
\begin{aligned}
x''(\tau) + 2\zeta\beta x'(\tau) + \beta^2 x(\tau) = & -2\xi\beta v_0 - \beta^2 x_s - \psi H(\omega_0 + \phi')\sum_{i=1}^{n}H(\delta_i)\delta_i \\
& - f_x H(v_0 + x')\sum_{i=1}^{n}H(\delta_i), \\
\phi''(\tau) + 2\kappa\phi'(\tau) + \phi(\tau) = & -2\kappa\omega_0 - \Phi_s - H(\omega_0 + \phi')\sum_{i=1}^{n}H(\delta_i)\delta_i \\
& - f_\phi H(v_0 + x')\mathrm{sgn}(\omega_0 + \phi')\sum_{i=1}^{n}H(\delta_i).
\end{aligned}
\tag{13}
$$

Meanwhile, the dimensionless depth of cut defined in Eq. (9) is transformed into

$$\delta_i = v_0\tau_i + x(\tau) - x(\tau - \tau_i), \quad i = 1, 2, \cdots, n, \tag{14}$$

and the implicit equation for the time delays, Eq. (10), becomes

$$\tau_i + \frac{\phi(\tau) - \phi(\tau - \tau_i)}{\omega_0} = \frac{\alpha_i}{\omega_0}, \quad i = 1, 2, \cdots, n. \tag{15}$$

2.3. Approximation of the state-dependent delays

Equation (15) does not have an analytical solution of the time delay as τ_i ($i = 1, 2, \cdots, n$) appears both in and out of $\phi(\tau - \tau_i)$, so we find an approximation of τ_i valid for small torsional deformation of the drill-string. Correspondingly, a small dimensionless parameter ν is introduced to denote $\phi(\tau)$ as $\nu\phi(\tau)$. Meanwhile, τ_i is expanded into

$$\tau_i = \tau_{i,0} + \nu\tau_{i,1} + \nu^2\tau_{i,2} + \cdots. \tag{16}$$

11

Next substituting Eq. (16) into Eq. (15), expanding $\nu\phi(\tau - \tau_i)$ into Taylor's series and collecting the coefficients of ν^0, ν^1 and ν^2 respectively yield

$$\tau_{i,0} = \frac{\alpha_i}{\omega_0}, \tag{17}$$

$$\tau_{i,1} + \frac{\phi(\tau) - \phi(\tau - \tau_{i,0})}{\omega_0} = 0, \tag{18}$$

and

$$\tau_{i,2} + \frac{\phi'(\tau - \tau_{i,0})}{\omega_0}\tau_{i,1} = 0. \tag{19}$$

Solving Eqs (17), (18) and (19) successively and using Eq. (16) yield the approximation of the time delay for the ith blade as follows

$$\tau_i = \frac{\alpha_i}{\omega_0} + \frac{\phi(\tau - \tau_{i,0}) - \phi(\tau)}{\omega_0} + \frac{\phi(\tau) - \phi(\tau - \tau_{i,0})}{\omega_0^2}\phi'(\tau - \tau_{i,0}) + \cdots. \tag{20}$$

It should be remarked that the approximation in Eq. (20) is valid only in the
120 vicinity of $\tau_i = \tau_{i,0}$ and can be used for static and linear analyses. In simulations of large-amplitude drilling vibration, this approximation is abandoned and Eq. (15) is solved by numerical iteration.

3. Stationary drilling process and its stability

With the dimensionless model and the approximation of regenerative delays
125 obtained above, next discussion focuses on linear drilling stability, where special attention is paid to the effects of number of blades and their distribution in the drill-bit. To begin with, the stationary drilling process is calculated, around which the governing equation is linearised for stability analysis by eigenvalue calculation. Namely, all the nonlinearity and non-smoothness are dropped first,
130 so that the analysis in this section is locally valid only. Then the selection of distribution angles is investigation, revealing that more blades with non-uniform distribution benefit the drilling stability.

12

3.1. Stationary drilling

When the drilling is stationary without any dynamic response ($x(\tau) = \phi(\tau) \equiv 0$), Eq. (20) is simplified to be

$$\tau_i \equiv \tau_{i,0} = \frac{\alpha_i}{\omega_0}, \quad i = 1, 2, \cdots, n, \tag{21}$$

and the nominal drilling depth given in Eq. (14) is fixed as

$$\delta_i \equiv \delta_{i,0} = v_0 \frac{\alpha_i}{\omega_0}, \quad i = 1, 2, \cdots, n, \tag{22}$$

where $\tau_{i,0}$ and $\delta_{i,0}$ denote the stationary dimensionless delay and drilling depth of the ith blade, respectively. Corresponding to the stationary cutting, the discontinuous functions are fixed as follows

$$
\begin{aligned}
H(\delta_i) &\equiv H(\delta_{i,0}) = 1, \\
H(\omega_0 + \phi') &= H(\omega_0) = 1, \\
H(v_0 + x') &= H(v_0) = 1, \\
\mathrm{sgn}(\omega_0 + \phi') &= \mathrm{sgn}(\omega_0) = 1.
\end{aligned}
\tag{23}
$$

As a result, the governing equation, Eq. (13), is simplified to be

$$
\begin{aligned}
0 &= -2\xi\beta v_0 - \beta^2 x_s - \psi \frac{v_0}{\omega_0} \sum_{i=1}^{n} \alpha_i - n f_x, \\
0 &= -2\kappa\omega_0 - \Phi_s - \frac{v_0}{\omega_0} \sum_{i=1}^{n} \alpha_i - n f_\phi.
\end{aligned}
\tag{24}
$$

Solving the above equation yield the dimensionless stationary drilling processes:

$$x_s = \frac{w_0}{\beta^2} \quad \text{and} \quad \Phi_s = t_0, \tag{25}$$

where $w_0 = -2\xi\beta v_0 - 2\pi\psi\frac{v_0}{\omega_0} - n f_x$ and $t_0 = -2\kappa\omega_0 - 2\pi\frac{v_0}{\omega_0} - n f_\phi$ are dimensionless static force and torque for the stationary drilling, respectively.

3.2. Critical boundaries

Stability of the stationary drilling process given in Eq. (25) can be revealed by eigenvalue analysis base on the linear part Eq. (13) [22]. From Eqs (14) and

13

(20), one can obtain linear approximation of the drilling depth of the ith blade as follows

$$\delta_i \approx \frac{v_0}{\omega_0}\alpha_i + \frac{v_0}{\omega_0}\left(\phi(\tau - \tau_{i,0}) - \phi(\tau)\right) + x(\tau) - x(\tau - \tau_{i,0}), \quad i = 1, 2, \cdots, n. \quad (26)$$

Moreover, Eq. (23) is still valid as the linear analysis is in the vicinity of the stationary state so that the non-smoothness would not play a role. Thus, submitting Eqs (23) and (26) into Eq. (13) yields the linearised governing equation as follows

$$\mathbf{I}\mathbf{x}''(\tau) + \mathbf{C}\mathbf{x}'(\tau) + \mathbf{K}\mathbf{x}(\tau) + n\mathbf{D}\mathbf{x}(\tau) - \mathbf{D}\sum_{i=1}^{n}\mathbf{x}(\tau - \tau_{i,0}) = 0, \qquad (27)$$

where

$$\mathbf{x}(\tau) = \begin{pmatrix} x(\tau) \\ \phi(\tau) \end{pmatrix}, \quad \mathbf{C} = \begin{pmatrix} 2\zeta\beta & 0 \\ 0 & 2\kappa \end{pmatrix},$$

$$\mathbf{K} = \begin{pmatrix} \beta^2 & 0 \\ 0 & 1 \end{pmatrix}, \quad \mathbf{D} = \begin{pmatrix} \psi & -\psi\frac{v}{\omega_0} \\ 1 & -\frac{v}{\omega_0} \end{pmatrix}. \qquad (28)$$

The corresponding characteristic equation of Eq. (27) is

$$\left| \mathbf{I}\lambda^2 + \mathbf{C}\lambda + \mathbf{K} + n\mathbf{D} - \mathbf{D}\sum_{i=1}^{n}\mathrm{e}^{-\lambda\tau_{i,0}} \right| = 0, \qquad (29)$$

or

$$\left(\lambda^2 + 2\zeta\beta\lambda + \beta^2\right)\left(\lambda^2 + 2\kappa\lambda + 1\right) - \frac{v_0}{\omega_0}\left(\lambda^2 + 2\zeta\beta\lambda + \beta^2\right)$$

$$\times \left(n - \sum_{i=1}^{n}\mathrm{e}^{-\lambda\tau_{i,0}}\right) + \psi\left(\lambda^2 + 2\kappa\lambda + 1\right)\left(n - \sum_{i=1}^{n}\mathrm{e}^{-\lambda\tau_{i,0}}\right) = 0, \qquad (30)$$

where $|\bullet|$ indicates the determinant and λ represents eigenvalues [27]. As known, the stable drilling requires all the eigenvalues having negative real parts but any positive real part indicates an unstable drilling process [28]. Thus the critical boundaries dividing the stable and unstable regions always have at least one pair of pure imaginary eigenvalues, $\lambda = \pm\omega\mathrm{i}$. Substituting this into Eq. (30), letting $v = \frac{v_0}{\omega_0}$, replacing $\tau_{i,0}$ by $\frac{\alpha_i}{\omega_0}$ and respectively collecting the real and

14

imaginary parts of the characteristic equation yield

$$
\begin{aligned}
&(\beta^2 - \omega^2)(1 - \omega^2) - 4\zeta\beta\kappa\omega^2 + 2\omega(v\zeta\beta - \kappa)\sum_{i=1}^{n}\sin\left(\frac{\alpha_i}{\omega_0}\omega\right) \\
&+ (1 - \omega^2 - v\beta^2 + v\omega^2)\left(n - \sum_{i=1}^{n}\cos\left(\frac{\alpha_i}{\omega_0}\omega\right)\right) = 0, \\
&2\zeta\beta\omega(1 - \omega^2) + 2\kappa\omega(\beta^2 - \omega^2) + 2\omega(\kappa - v\zeta\beta)\left(n - \sum_{i=1}^{n}\cos\left(\frac{\alpha_i}{\omega_0}\omega\right)\right) \\
&+ (1 - \omega^2 - v\beta^2 + v\omega^2)\sin\left(\frac{\alpha_i}{\omega_0}\omega\right) = 0.
\end{aligned}
\tag{31}
$$

Solving Eq. (31) yields the critical boundaries for the drilling stability, but this transcendental equation is unlike the one studied in [14] which has only an unique time delay. Equation (31) has n distinct delays, significantly complicat-
ing the calculation of eigenvalues, so the following analysis will employ numerical iterations and continuation scheme [22] to obtain the critical boundaries.

3.3. Angle constraint

Given the significance of time delays for various systems [29, 30, 31, 32], the selection of rotary speed, ω_0, and angles between successive blades, α_i ($i = 1, 2, \cdots, n$), which determines the combination of the time delays, $\tau_{i,0}$ ($i = 1, 2, \cdots, n$), becomes very critical for the drilling stability. Moreover, it is known from the commutative property of addition and the governing equations of the drilling dynamics, Eqs. (13) and (27), that it is not the permutation but only the combination of the angles, α_i ($i = 1, 2, \cdots, n$), influencing the drilling stability and dynamics. That is to say, there would be no difference if we randomly reorganise the blade distribution in Fig. 3(a) into that in Fig. 3(b) provided they have the same combination of the angles.

Therefore, we can sort the angles as follows without loss of generality for the analysis of the drilling dynamics

$$
0 \leq \alpha_n \leq \cdots \leq \alpha_{i+1} \leq \alpha_i \leq \cdots \leq \alpha_2 \leq \alpha_1.
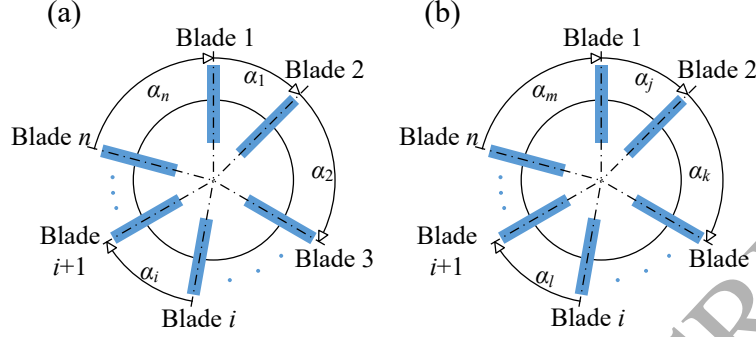\tag{32}
$$

15

Figure 3: Two different permutations of the blade distribution, making no difference for the drilling dynamics as long as the combination of the angles are the same.

In addition, it is also seen from Fig. 3 that

$$\sum_{i=1}^{n} \alpha_i = 2\pi. \tag{33}$$

From Eqs (32) and (33), one can obtain that

$$\frac{2\pi}{n} = \frac{\sum_{i=1}^{n} \alpha_i}{n} \leq \alpha_1 = 2\pi - \sum_{i=2}^{n} \alpha_i \leq 2\pi. \tag{34}$$

In a similar manner, the constraint for a_2 can be represented as

$$\frac{2\pi - \alpha_1}{n - 1} = \frac{\sum_{i=2}^{n} \alpha_i}{n - 1} \leq \alpha_2 = 2\pi - \sum_{i=3}^{n} \alpha_i - \alpha_1 \leq 2\pi - \alpha_1. \tag{35}$$

Given Eq. (32), this constraint is rewritten as

$$\frac{2\pi - \alpha_1}{n - 1} \leq \alpha_2 \leq \min\left(\alpha_1, 2\pi - \alpha_1\right). \tag{36}$$

By repeating this procedure, one can find the constraints for all the angles as follows

$$\frac{2\pi}{n} \leq \alpha_1 \leq 2\pi,$$
$$\frac{2\pi - \sum_{j=1}^{i-1} \alpha_j}{n - i + 1} \leq \alpha_i \leq \min\left(\alpha_{i-1}, 2\pi - \sum_{j=1}^{i-1} \alpha_j\right), \quad i = 2, 3 \cdots, n - 1, \tag{37}$$
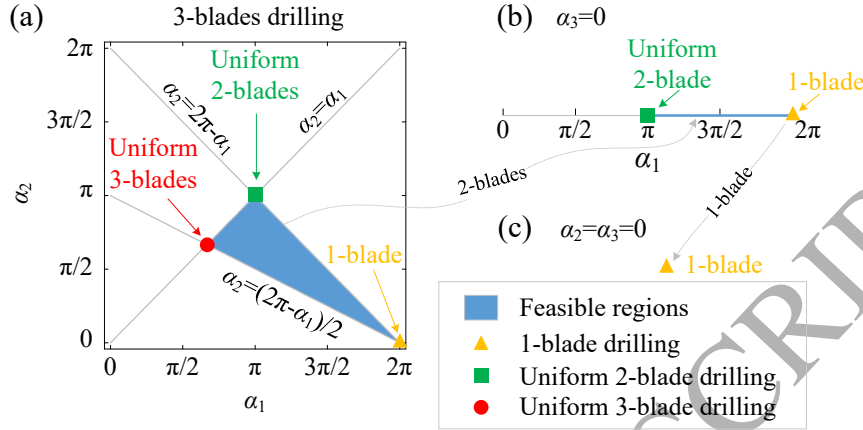$$\alpha_n = 2\pi - \sum_{i=1}^{n-1} \alpha_i.$$

16

Figure 4: Constraints of the angles' selection for (a) 3-blades, (b) 2-blades and (c) 1-blade drilling, where only the blue regions are feasible for design.

For the analysis of drilling dynamics with n-blades, the constraint in Eq. (37) can shrink the feasible region for the selection of the angles combination. To illustrate, the feasible regions of the angles for 2- and 3-blades drilling shrink to be

$$\alpha_1 \in \left[\frac{2\pi}{2}, 2\pi\right], \quad \alpha_2 = 2\pi - \alpha_1, \tag{38}$$

and

$$\begin{aligned} &\alpha_1 \in \left[\frac{2\pi}{3}, 2\pi\right], \\ &\alpha_2 \in \left[\frac{2\pi - \alpha_1}{2}, \min\left(\alpha_1, 2\pi - \alpha_1\right)\right], \\ &\alpha_3 = 2\pi - \alpha_1 - \alpha_2, \end{aligned} \tag{39}$$

respectively. The two cases are displayed in Fig. 4, where the areas for the selection of the distribution angles are marked as blue, which are extensively smaller than those without sorting the angles according to Eq. (32).

Degenerate model. In addition, the extreme cases marked in Fig. 4 represent the degenerate situations. For example, the yellow triangles in Figs 4(a) and (b) have $\alpha_1 = 2\pi$, which actually becomes an 1-blade drilling shown in Fig. 4(c). In a similar manner, the line segment between the yellow triangle and the green

17

Table 1: Values of dimensionless parameters adopted from [14]

Parameter	Symbol	Value [-]
Axial damping coefficient	ζ	0.01
Torsional damping coefficient	κ	0.01
Axial-to-torsional frequency ratio	β	1.58
Cutter inclination parameter	ψ	13.9
Frictional WOB	f_x	1.74048
Frictional TOB	f_ϕ	0.04467

square in Fig. 4(a) for the 3-blades drilling has $\alpha_1 + \alpha_2 = 2\pi$ and $\alpha_3 = 0$, which is exactly the same as the blue segment in Fig. 4(b) for the non-uniform 2-blades drilling. Both of the green squares in Figs 4(a) and (b) have $\alpha_1 = \alpha_2 = \pi$, indicating the uniform 2-blades drilling, while another uniform case is the red disk in Fig. 4(a) for 3-blades drilling [14, 26]. From this viewpoint, this complex model proposed here can degenerate into a relatively simpler problem in two ways: the n-blades drilling becomes $(n-1)$-blades drilling when $\alpha_n = 0$, while the non-uniform case degenerates into uniform once all the angles are identical.

3.4. Numerical eigenvalue analysis

With the non-uniformly distributed n blades, the drilling dynamics is normally governed by equations with n distinct time delays, which extensively complicates the analysis of the drilling stability so that analytically solving Eq. (30) is impossible. Therefore, the following analysis will use numerical method based on Newton-Raphson iteration and continuation scheme [22]. Moreover, it is known from Fig. 4 that part of the n-blades drilling dynamics is known once the $(n-1)$-blades problem has been solved, so the following analysis will successively discuss the stability of drilling operations with 1, 2 and 3 blades.

3.4.1. 1-blade drilling stability

The linear stability analysis is started with the simplest 1-blade drilling. By using the parameter values listed in Table 1, one obtains the stability boundaries

18

in Fig. 5(a), dividing the stable (grey) and unstable (white) regions. To validate
the stability chart, one point inside the stable ($\omega_0 = 15$ and $v = 0.5$) is selected
to show the focus in Fig. 5(b), where both the axial and torsional vibration
gradually damped down. When the parameter value crosses the left boundary,
as seen in Fig. 5(c) for $\omega_0 = 9$ and $v = 0.5$, unstable drilling with large-amplitude
axial vibration occurs, where the non-smoothness only in the downward bit
progression presents as bit-bounce. By contrast, when the parameter selection
is above the stability boundary, Fig. 5(d) shows us non-smoothness both in the
axial and in the torsional movements. Details of Fig. 5(d) is enlarged in Fig. 5(e),
showing that the axial stick motion is always in advance of the bit-bounce.
Once the torsional movement of the drill-bit is stuck, the axial progression
is accelerated forward and then backward for bit-bounce. When the drill-bit
bounces backwards, the torsional deformation of the drill-string is released for
the slip motion until the torsional movement gets stuck again. It illustrates that
the source of drilling instability in this area is in the torsional movement.

3.4.2. 2-blades drilling stability

Then we move forward to the case of 2-blades drilling, which introduces
flexibility in the angles' selection and thus the time delays for the improvement
of drilling stability. As discussed in Section 3.3, $\alpha_1 = \pi$ and 2π respectively
correspond with the uniform drilling studied by Nandakumar and Wiercigroch
[14] and the 1-blade drilling discussed above. By using the non-uniform drilling,
we expect to properly select $\alpha_1 \in (\pi, 2\pi)$ for the largest stable region. As
displayed in Fig. 6(a), the stable region expands monotonously with respect to
the increase of α_1 from π (uniform drilling) to $\frac{15\pi}{10}$. Then the stable region in
Fig. 6(b) gradually shrinks with respect to further increase of α_1 to 2π (1-blade
drilling). Namely, the largest stable region of the 2-blades drilling is achieved
by using $\alpha_1 = \frac{3\pi}{2}$ and $\alpha_2 = \frac{\pi}{2}$, instead of the conventional uniform drilling.
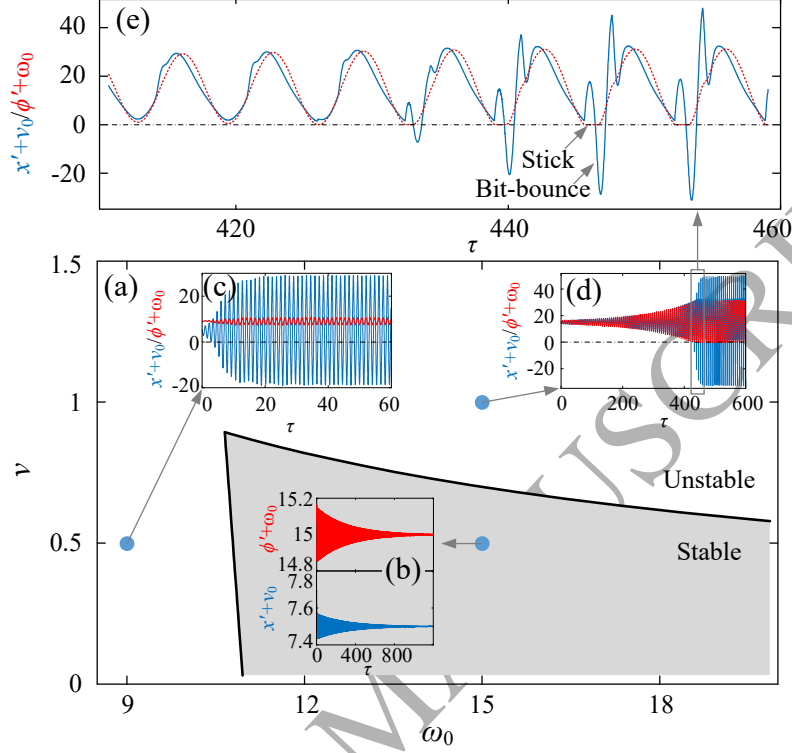
19

Figure 5: (a) Stability boundaries of 1-blade drilling, with time series of (b) stable drilling for $\omega_0 = 15$ and $v = 0.5$, (c) bit-bounce for $\omega_0 = 9$ and $v = 1$ and (d) stick-slip for $\omega_0 = 15$ and $v = 1$ added. In addition, part of the stick-slip motion in Panel (d) is enlarged in Panel (e).
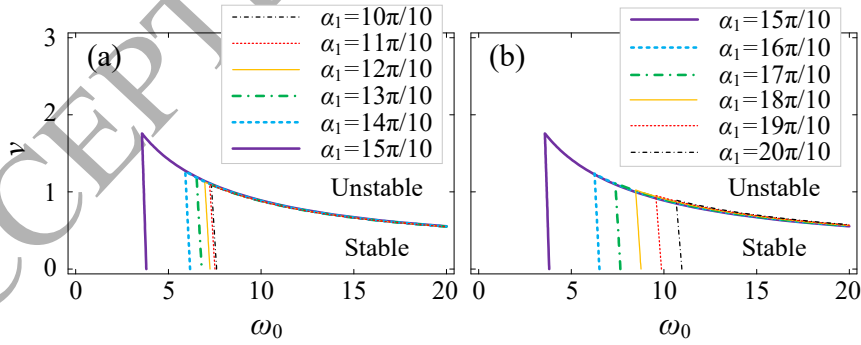

Figure 6: Stability boundaries of 2-blades drilling for various values of α_1, yielding the largest stable region for $\alpha_1 = \frac{15\pi}{10}$. By contrast, the uniform-distributed drilling ($\alpha_1 = \frac{10\pi}{10}$) and 1-blade drilling ($\alpha_1 = \frac{20\pi}{10}$) have smaller stable regions.
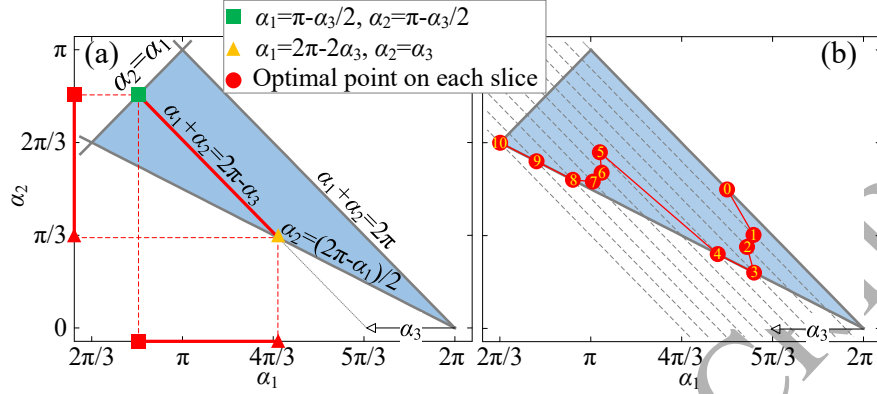
Figure 7: (a) Feasible angles for the 3-blades drilling. For every fixed value of $\alpha_3 \in [0, \frac{2\pi}{3}]$, the feasible values of α_1 and α_2 are located on the red line segment ($\alpha_1 + \alpha_2 = 2\pi - \alpha_3$) between the green square ($\alpha_1 = \alpha_2 = \pi - \alpha_3/2$) and the yellow triangle ($\alpha_1 = 2\pi - 2\alpha_3$ and $\alpha_2 = \alpha_3$). (b) Trace of the optimal point for the largest stable region for every given value of α_3.

3.4.3. 3-blades drilling stability

The case of 3-blades drilling is even more complex as two parameters out of α_1, α_2 and α_3 should be determined before the stability analysis. The feasible region for the angles' selection has already been displayed in Fig. 4(a), where the right edge of the feasible region corresponding to 2-blades drilling has been thoroughly studied in the previous section, so the analysis will move from this edge towards its opposite corner corresponding to uniform 3-blades drilling.

This procedure is schematically illustrated in Fig. 7(a), where we draw the line, $\alpha_1 + \alpha_2 = 2\pi - \alpha_3$, for a given value of α_3. This line has the segment (red) between the green square and the yellow triangle located in the feasible region. With respect to the increase of α_3 from 0 to $\frac{2\pi}{3}$, the line segment correspondingly sweeps all the feasible region from the edge for 2-blades drilling to the corner for uniform 3-blades drilling. By using some simple algebraic manipulation, one can project the red linear segment onto the horizontal and vertical coordinates for the selection of α_1 and α_2 as follows

$$\alpha_1 \in [\pi - \frac{\alpha_3}{2}, 2\pi - 2\alpha_3], \quad \alpha_2 = 2\pi - \alpha_1 - \alpha_3, \tag{40}$$
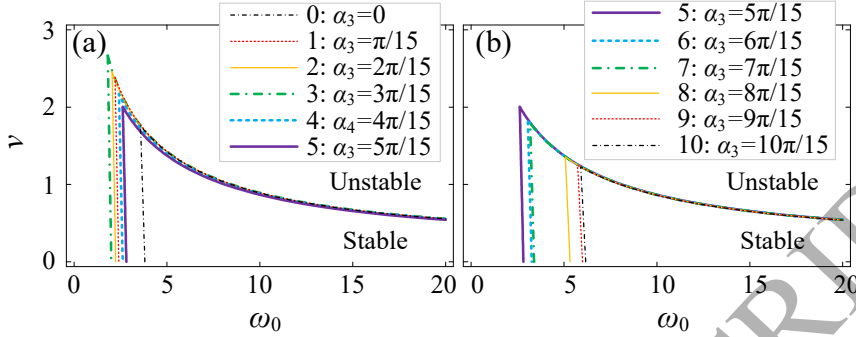
21

Figure 8: Stability boundaries of drilling with distribution angles corresponding to the optimal points on (a) Slices 0-5 and (b) Slices 5-10 plotted in Fig. 7, showing the largest stable region on the 3rd slice.

where $\alpha_3 \in [0, \frac{2\pi}{3}]$.

By following the procedure described above, one can change the complex 3-blades drilling problem into a relative simpler 2-blades problem for a given value of α_3. As illustrated in Fig. 7(b), the feasible region is sliced into 11 pieces and the jth slice has $\alpha_3 = \frac{j\pi}{15}$ ($j = 0, 1, \cdots, 10$), where Slices 0 and 10 correspond to 2-blades and uniform 3-blades drilling operations, respectively. For any given value of α_3, one can repeat the analysis in Section 3.4.2 to find the optimal point on the corresponding slice. As shown Fig. 7(b), the optimized points on every slices are tracked and marked as red dots. Then the stability charts corresponding with every optimal points in Fig. 7(b) are compared in Figs 8(a) and (b), showing the largest stable region in Fig. 8(a) for $\alpha_3 = \frac{3\pi}{15}$ (dot-dashed green line). This region corresponds with the 3rd slice in Fig. 7(b), where the location of the 3rd red dot has $\alpha_1 = \frac{8\pi}{5}$ and $\alpha_2 = \frac{\pi}{5}$.

3.4.4. Further discussion

The numerical discussion in the above sections shows that the i-blades problem can be recursively divided into a series of $(i-1)$-blades drilling dynamics, and the $(i-1)$-blades drilling can be regarded as a special case of i-blades drilling. For example, the 4-blades drilling dynamics can be divided into a series of 3-blades problems which has already been studied in Section 3.4.3, which
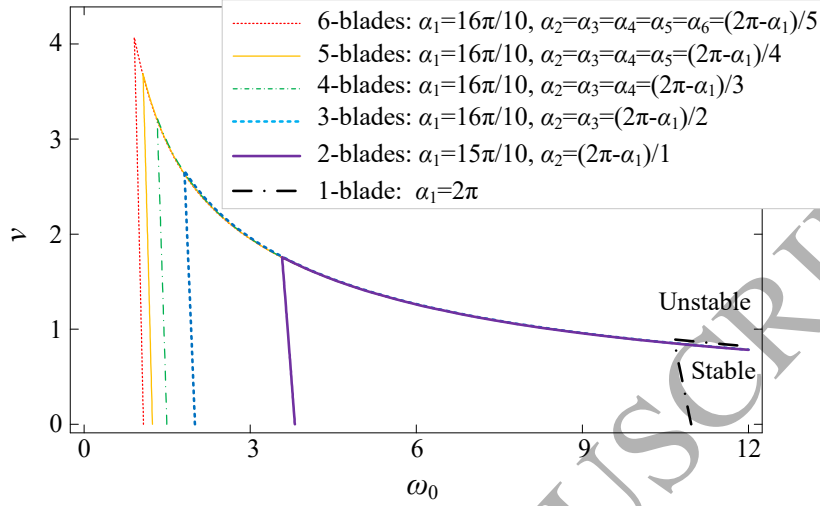
Figure 9: Enlargement of the stable regions by using more blades in the drill-bit.

can be further divided into several series of 2-blades drilling dynamics discussed in Section 3.4.2. Correspondingly, the tediousness of this discussion will grow

235 exponentially when more and more blades are used in the drill-bit, although it is possible to write a recursive algorithm for the problem of drilling with many blades.

To avoid the tediousness, we can make a guess about the optimal selection of the angles based on the results obtained in the above sections. The optimal

240 combinations of the angles for 2- and 3-blades drilling are $\alpha_1 = \frac{15\pi}{10}$ and $\alpha_2 = \frac{5\pi}{10}$, and $\alpha_1 = \frac{16\pi}{10}$ and $\alpha_2 = \alpha_3 = \frac{2\pi}{10}$, respectively, both of which have the largest angle, α_1, occupies the majority of the angles' summation, around 80% of 2π. Thus, as displayed in Fig. 9, we fixed α_1 as $\frac{16\pi}{10}$ and let the rest of the angles equally share $2\pi - \alpha_1$ for drilling with more than 2 blades. As seen, the stable

245 region expands monotonously with respect to the increase of the blade number, but the benefit of adding an extra blade keeps decreasing.
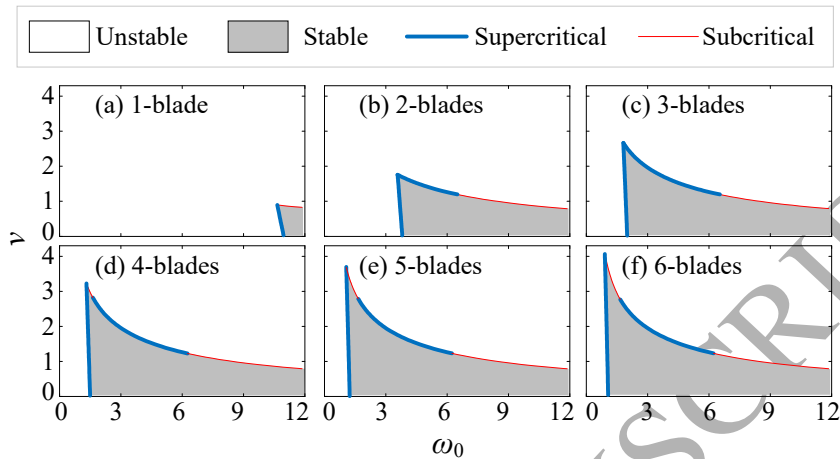
23

Figure 10: Criticality of the Hopf bifurcation on the stability boundaries of (a) 1-blade, (b) 2-blades, (c) 3-blades, (d) 4-blades, (e) 5-blades and (f) 6-blades drilling processes.

4. Perturbation and numerical analysis

When the parameters cross the boundaries in Fig. 9 to enter the unstable region, periodic drilling vibration is incurred by Hopf bifurcation, which could be either subcritical or supercritical [33, 34]. In addition to the local bifurcation, its global bifurcation is also very crucial since it introduces various complex drilling dynamics and co-existing attractors significantly influencing drilling operations.

4.1. Analytical perturbation analysis

The same as other cutting processes, such as turning [35], milling [36] and grinding [22] operations, the subcritical Hopf bifurcation bends the periodic branch back into the stable region, yielding unsafe zones (UZs) for the co-existence of stable and unstable drilling operations. To avoid the UZs which hazards the stable drilling operations near the subcritical stability boundaries, the criticality of Hopf bifurcation born on the drilling stability boundaries can be checked by perturbation methods, such as the method of multiple scales (MMS) [37]. A brief perturbation analysis of 1-blade drilling is given in Appendix A, and one can refer to [38, 39] for more details.

24

Results of the perturbation analysis is displayed in Fig. 10, illustrating the criticality of the Hopf bifurcation on the stability boundaries displayed in Fig. 9 with the thin red and thick blue lines representing the subcritical and super-critical Hopf bifurcations, respectively. It is seen that the left boundary of the stable region is always of supercritical instability, no matter how many blades are employed. By contrast, the nonlinear property of the top boundary keeps varying with respect to the addition of a new blade. It is always subcritical in Fig. 10(a) for 1-blade drilling, while the left segments of the top boundary in Figs 10(b) and (c) become supercritical when the stable region extends leftwards for 2- and 3-blades drilling. Then, the 4-, 5- and 6-blades drilling operations introduce one more subcritical segment on the left end of the top boundaries shown in Figs 10(d), (e) and (f). This phenomenon gives a warning that the drilling operates at the top-left corner of the stable region can be very dangerous when more than 3-blades are used. In addition, as the right parts of all the top boundaries in Fig. 10 are subcritical, drilling with $\omega_0 > 6$ should keep a distant with the stability boundary to avoid the co-existing large-amplitude vibration.

4.2. Numerical bifurcation analysis

Next the local bifurcation analysis will be extended by numerical simulations, with the boundaries in Fig. 10(c) for 3-blades drilling chosen as examples. The first case has ω_0 fixed as 8 and v varying between 0.8 and 4 to cross the top subcritical stability boundary. With the Poincaré section selected as $\tau_1 = \tau_{1,0}$ and $\tau_1' > 0$ and the value of x on the section denoted as x^*, one obtains the bifurcation diagram shown in Fig. 11, where the red and blue dots in Fig. 11(a) represent the result from forward and backward simulations, respectively. As seen, the subcritical Hopf bifurcation occurs for $v = 1.04$, yielding co-existence of stable drilling and periodic chatter for $v \in [0.94, 1.04]$. To illustrate, time series and phase portrait for $v = 1$ are illustrated in Figs 11(b) and (c), where the drilling chatter in Fig. 11(c) has non-smoothness in axial and torsional speeds and cutting depth $\delta_2 = \delta_3$, i.e., it is of bit-bounce, stick-slip motion and loss of contact in the second and third blades. This periodic chatter persists for
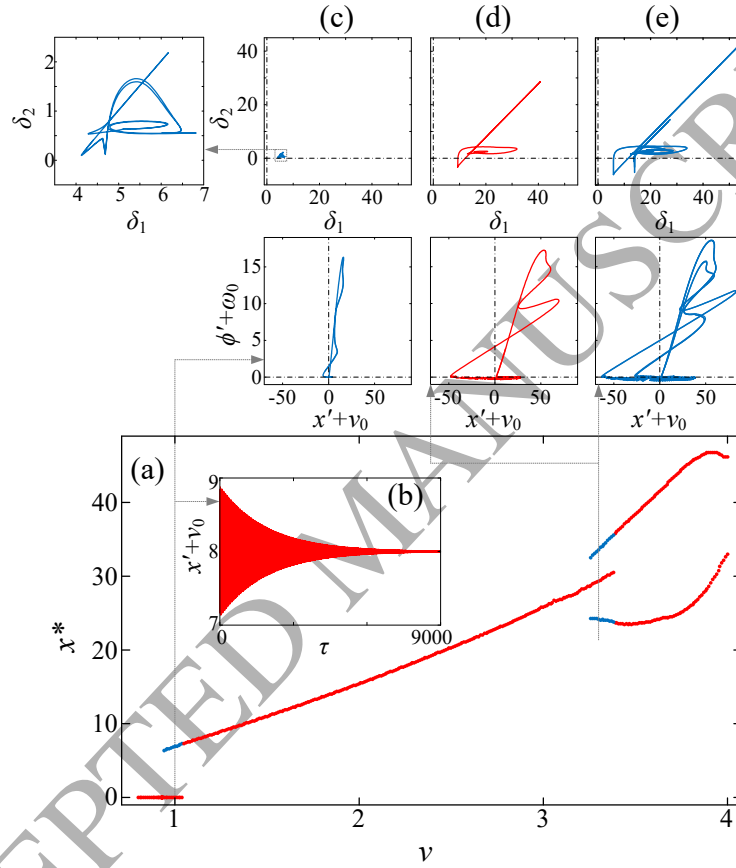
25

Figure 11: (a) Bifurcation diagram for 3-blades drilling with $\omega_0 = 8$ and $v \in [0.8, 4]$. The subcritical Hopf bifurcation at $v = 1.04$ results in co-existence of stationary drilling and chatter with stick-slip motion at (b-c) $v = 1$. As shown in Panels (d-e) $v = 3.3$, the chatter then jumps to a periodic-two branch, after they co-exist for $v \in [3.26, 3.38]$.

26

$v < 3.38$ where it jumps to another periodic-two chatter. In addition, as shown in Figs. 11(d) and (e), the two chatter motions co-exist for $v \in [3.26, 3.38]$.

295 The second case focuses on the supercritical instability on the top boundary, where ω_0 is fixed as 3 and v varies between 1.2 and 4. Bifurcation diagram in Fig. 12(a) shows supercritical Hopf bifurcation for $v = 1.96$, which transforms the stable drilling shown in Fig. 12(b) for $v = 1.5$ into the periodic chatter in Fig. 12(d) for $v = 2$. The amplitude of this periodic chatter is relative 300 small without non-smoothness in its phase portrait, but it is then gradually enhanced by the increase of v, and bit-bounce and stick-slip motions show up for $v > 2.07$. It is shown in Figs 12(c) and (e) that the new chatter motion with non-smoothness in the axial and torsional speeds persists with respect to the decrease of v, which co-exists with the stable drilling or small-amplitude chatter 305 for $v \in [1.36, 2.07]$. With respect to the increase of v, this periodic motion still persists until periodic doubling occurs for $v = 3.59$, yielding the periodic-two chatter for $v = 3.8$ shown in Fig. 12(f). Unlike the chatter motions displayed in Fig. 11, it is worth noting that all the drilling dynamics in Fig. 12 has only the phenomena of bit-bounce and stick-motion, without loss of blade-rock contact.

310 The third case studies the nonlinear oscillations on the left side of the stable region of 3-blades drilling, where v is fixed as 1 and ω_0 gradually decreases from 2 to 0.1. As shown in Fig. 13(a), this bifurcation pattern is much more complex compared with the two preceding cases. With respect to the decrease of ω_0, the stable drilling bifurcates into small-amplitude periodic chatter for 315 $\omega_0 \in [1.9308, 1.932]$ via supercritical Hopf bifurcation, which is demonstrated by the phase portrait for $\omega_0 = 1.931$ in Fig. 13(l). As illustrated in Figs. 13(k) and (i), this periodic motion is then bifurcates into quasi-periodic with bit-bounce for $\omega_0 < 1.9306$ and then loss of contact in the blades shows up for $\omega_0 < 1.66$. In addition, another periodic chatter with bit-bounce and stick-slip 320 motion co-exists with the quasi-periodic for $\omega_0 \in [1.39, 1.77]$. For $\omega_0 < 1.39$, the quasi-periodic one disappears but the periodic one persist until it changes into irregular before it jumps to another periodic branch for $\omega_0 < 1.04$, which is of bit-bounce, stick-slip motion and loss of contact. As seen in Figs. 13(g)
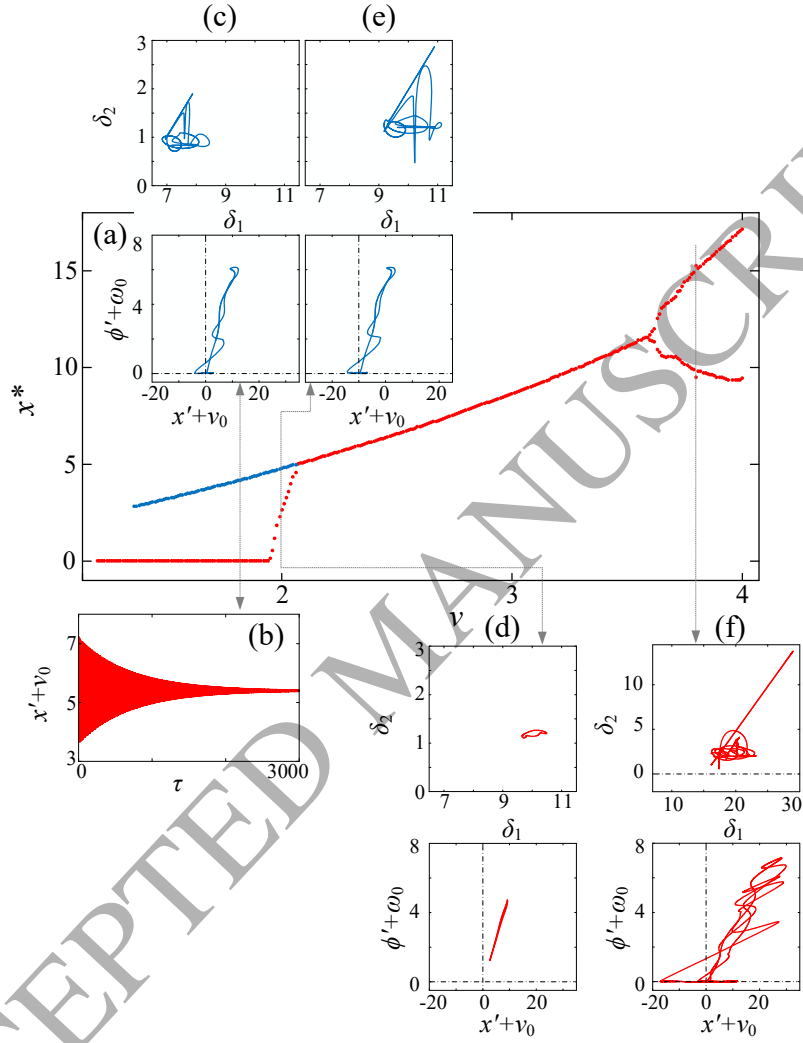
27

Figure 12: (a) Bifurcation diagram for 3-blades with $\omega_0 = 3$ and $v \in [1.2, 4]$ shows a supercritical Hopf bifurcation at $v = 1.96$, incurring small-amplitude chatter without non-smoothness. However, stick-slip motion turns up at $v = 2.07$, resulting in a large-amplitude chatter co-existing with the stationary drilling and small-amplitude chatter for (b-c) $v = 1.5$ and (e-d) $v = 2$. The large-amplitude chatter then undergoes periodic-doubling for $v = 3.59$, resulting periodic-two motion for (f) $v = 3.8$.
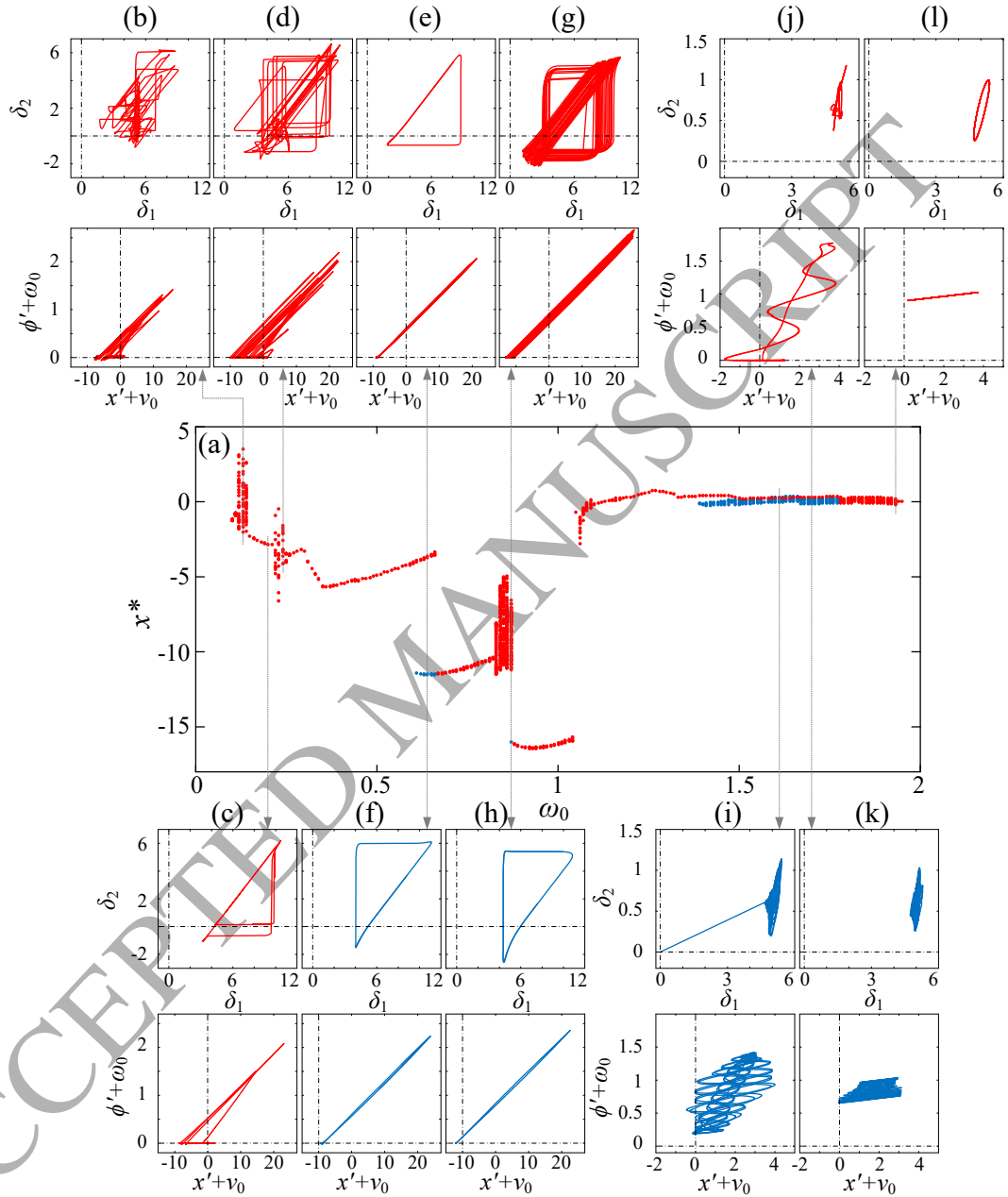
28

Figure 13: (a) Bifurcation diagram for 3-blades drilling with $v = 1$ and $\omega_0 \in [0.1, 2]$. Periodic chatter for (l) $\omega_0 = 1.931$ becomes quasi-periodic bit-bounce co-existing with stick-slip motion for (j-k) $\omega_0 = 1.7$. Chatter with loss of blade-rock contact, shown in (i) $v = 1.6$, turns up for $v < 1.66$, which disappears at $\omega_0 = 1.39$, leaving the periodic undergoes several jumps for various complex drilling dynamics for (g-h) $v = 0.87$, (e-f) 0.64, (d) 0.24, (c) 0.2 and (b) 0.13.

and (h), this branch then jumps to another irregular motion for $\omega_0 < 0.87$,

which suddenly changes into another periodic chatter for $\omega_0 < 0.82$. For further

decrease of ω_0, the periodic branch then jumps to another one for $\omega_0 < 0.6$, with

a bistable region for $\omega_0 \in [0.61, 0.66]$ for the co-existence of the two periodic

branches. The new periodic branch persists with respect to further decrease

of ω_0 until irregular and periodic-two chatter found for $\omega_0 < 0.26$. In general,

low torsional speed, ω_0, induces more complex drilling dynamics with various

non-smoothness in axial and torsional speeds and blade-rock interactions.

5. Conclusions

By using the lumped parameter model involving axial and torsional defor-

mations of the drill-string, we have investigated the stability and dynamics of

drilling process with non-uniformly distributed blades. It has been found that

the non-uniform distribution can enlarge the region for stable drilling and the

introduction of an extra blade in the drill-bit can further enhance the drilling

stability. In addition, nonlinear bifurcation analysis based the MMS has found

both subcritical and supercritical types of drilling instabilities, where the sub-

critical one undermines the benefit of the top-left corner and top-right part of

the stable regions of drilling operations with more than 3 blades.

Firstly, a lumped parameter model of the drill-string was proposed to study

the coupled axial-torsional vibration, with both regenerative and frictional bit-

rock interactions regarded as the sources of drilling instability. Moreover, the

model involves the non-smoothness in the bit-rock interaction for the study of

nonlinear drilling dynamics. To analyse the effect of drill-bit with non-uniformly

distributed blades, every angles between successive blades and their correspond-

ing time delays were regarded as independent parameters, resulting in a more

complex model compared with previous investigations on uniform drilling.

Then the linear eigenvalue analysis for the drilling stability was performed to

study the effects of blade number and the angle distribution on the stable region.

By sorting the angles, the feasible region of angles' selection was largely shrunk

30

to simplify the eigenvalue analysis. It was found that the $(i-1)$-blades drilling can be deemed as a special case of the i-blades drilling, or the investigation of the dynamics of drilling with j blades can be divided into a bunch of $(j-1)$-blades drilling dynamics. Eigenvalue analysis revealed that the non-uniformed distribution of the blades can improve the drilling stability, and the best drill-bit has one blade occupy the majority of the summation of the angles, around 80% of 2π. Moreover, it was found that the drilling stability can also be enhanced by introducing more blades, but the improvement becomes less and less evident.

Next the perturbation analysis based on the MMS found both subcritical and supercritical Hopf bifurcation on the stability boundaries. It was observed that the left boundaries of the stable region is always supercritical, no matter how many blades are involved. By contrast, the criticality of the Hopf bifurcation on the top boundaries crucially depends on the number of blades in the drill-bit. Given the properties of the subcritical type of Hopf bifurcation, we suggested that the areas near the top-left corner and the top-right part of the stable regions should be avoided to guarantee the drilling stability.

Finally, numerical simulations were used for nonlinear bifurcation analysis, yielding various drilling chatters. In general, the bifurcation pattern with respect to the decrease of torsional speed is much more complex compared with that with respect to the increase of axial speed. It was also seen that the non-smoothness in the axial and torsional speeds and blade-rock interaction significantly shapes the nonlinear drilling dynamics, where the phenomena of bit-bounce, stick-slip motion, loss of contact and multi-stability were observed.

Appendix A. Nonlinear analysis by MMS

The criticality of Hopf bifurcation on the stability boundary of 1-blade drilling is discussed as an example, and the analysis of drilling with more blades is straightforward. The method of multiple scales (MMS) [38] introduces time

31

scales, $T_0 = \tau$ and $T_2 = \epsilon^2 \tau$, and expands $\mathbf{x}(\tau)$ into

$$\mathbf{x}(\tau) = \epsilon \mathbf{x}_1(T_0, T_2) + \epsilon^2 \mathbf{x}_2(T_0, T_2) + \epsilon^3 \mathbf{x}_3(T_0, T_2) + \cdots$$

$$= \epsilon \begin{pmatrix} x_1(T_0, T_2) \\ \phi_1(T_0, T_2) \end{pmatrix} + \epsilon^2 \begin{pmatrix} x_2(T_0, T_2) \\ \phi_2(T_0, T_2) \end{pmatrix} + \epsilon^3 \begin{pmatrix} x_3(T_0, T_2) \\ \phi_3(T_0, T_2) \end{pmatrix} + \cdots. \qquad \text{(A.1)}$$

Given the approximation of the state-dependent delay in Eq. (20), the delayed terms are expanded into Taylor's series as follows

$$
\begin{aligned}
x(\tau - \tau_1) =& \epsilon x_1(T_0 - \tau_1, T_2 - \epsilon^2 \tau_1) + \epsilon^2 x_2(T_0 - \tau_1, T_2 - \epsilon^2 \tau_1) \\
&+ \epsilon^3 x_3(T_0 - \tau_1, T_2 - \epsilon^2 \tau_1) + \cdots \\
=& \epsilon x_1(T_0 - \tau_{1,0}, T_2) + \epsilon^2 \bigg(x_2(T_0 - \tau_{1,0}, T_2) \\
&+ \frac{\phi_1(T_0, T_2) - \phi_1(T_0 - \tau_{1,0}, T_2)}{\omega_0} \frac{\partial x_1(T_0 - \tau_{1,0}, T_2)}{\partial T_0} \bigg) \\
&+ \epsilon^3 \bigg(x_3(T_0 - \tau_{1,0}, T_2) - \tau_{1,0} \frac{\partial x_1(T_0 - \tau_{1,0}, T_2)}{\partial T_2} \\
&+ \frac{\phi_1(T_0, T_2) - \phi_1(T_0 - \tau_{1,0}, T_2)}{\omega_0} \frac{\partial x_2(T_0 - \tau_{1,0}, T_2)}{\partial T_0} \\
&+ \frac{\phi_2(T_0, T_2) - \phi_2(T_0 - \tau_{1,0}, T_2)}{\omega_0} \frac{\partial x_1(T_0 - \tau_{1,0}, T_2)}{\partial T_0} \\
&- \frac{\phi_1(T_0, T_2) - \phi_1(T_0 - \tau_{1,0}, T_2)}{\omega_0^2} \frac{\partial \phi_1(T_0 - \tau_{1,0}, T_2)}{\partial T_0} \frac{\partial x_1(T_0 - \tau_{1,0}, T_2)}{\partial T_0} \\
&+ \frac{(\phi_1(T_0, T_2) - \phi_1(T_0 - \tau_{1,0}, T_2))^2}{2\omega_0^2} \frac{\partial^2 x_1(T_0 - \tau_{1,0}, T_2)}{\partial T_0^2} \bigg) + \cdots, \\
\phi(\tau - \tau_1) =& \epsilon \phi_1(T_0 - \tau_{1,0}, T_2) + \epsilon^2 \bigg(\phi_2(T_0 - \tau_{1,0}, T_2) \\
&+ \frac{\phi_1(T_0, T_2) - \phi_1(T_0 - \tau_{1,0}, T_2)}{\omega_0} \frac{\partial \phi_1(T_0 - \tau_{1,0}, T_2)}{\partial T_0} \bigg) \\
&+ \epsilon^3 \bigg(\phi_3(T_0 - \tau_{1,0}, T_2) - \tau_{1,0} \frac{\partial \phi_1(T_0 - \tau_{1,0}, T_2)}{\partial T_2} \\
&+ \frac{\phi_1(T_0, T_2) - \phi_1(T_0 - \tau_{1,0}, T_2)}{\omega_0} \frac{\partial \phi_2(T_0 - \tau_{1,0}, T_2)}{\partial T_0} \\
&+ \frac{\phi_2(T_0, T_2) - \phi_2(T_0 - \tau_{1,0}, T_2)}{\omega_0} \frac{\partial \phi_1(T_0 - \tau_{1,0}, T_2)}{\partial T_0} \\
&- \frac{\phi_1(T_0, T_2) - \phi_1(T_0 - \tau_{1,0}, T_2)}{\omega_0^2} \frac{\partial \phi_1(T_0 - \tau_{1,0}, T_2)}{\partial T_0} \frac{\partial \phi_1(T_0 - \tau_{1,0}, T_2)}{\partial T_0} \\
&+ \frac{(\phi_1(T_0, T_2) - \phi_1(T_0 - \tau_{1,0}, T_2))^2}{2\omega_0^2} \frac{\partial^2 \phi_1(T_0 - \tau_{1,0}, T_2)}{\partial T_0^2} \bigg) + \cdots.
\end{aligned}
$$

$$(A.2)$$

Then, substituting Eqs (A.1) and (A.2) into Eq. (13) and collecting the

coefficients of ϵ and ϵ^2 yield

$$\mathbf{I}\frac{\partial^2 \mathbf{x}_1(T_0, T_2)}{\partial T_0^2} + \mathbf{C}\frac{\partial \mathbf{x}_1(T_0, T_2)}{\partial T_0} + (\mathbf{K} + \mathbf{D})\mathbf{x}_1(T_0, T_2) - \mathbf{D}\mathbf{x}_1(T_0 - \tau_{1,0}, T_2) = 0,$$

$$(A.3)$$

and

$$\mathbf{I}\frac{\partial^2 \mathbf{x}_2(T_0, T_2)}{\partial T_0^2} + \mathbf{C}\frac{\partial \mathbf{x}_2(T_0, T_2)}{\partial T_0} + (\mathbf{K} + \mathbf{D})\mathbf{x}_2(T_0, T_2) - \mathbf{D}\mathbf{x}_2(T_0 - \tau_{1,0}, T_2) = \mathbf{N}_2,$$

$$(A.4)$$

where

$$\mathbf{N}_2 = \begin{pmatrix} \psi \\ 1 \end{pmatrix} \frac{(\phi_1(T_0, T_2) - \phi_1(T_0 - \tau_{1,0}, T_2))\left(\frac{\partial x_1(T_0 - \tau_{1,0}, T_2)}{\partial T_0} - v_c\frac{\partial \phi_1(T_0 - \tau_{1,0}, T_2)}{\partial T_0}\right)}{\omega_0}.$$

$$(A.5)$$

Equation (A.3) is the same as the linearised governing equation, Eq. (27), which has the non-decaying solution corresponding to the critical eigenvalues, $\lambda = \pm i\omega$, as follows

$$\mathbf{x}_1 = \begin{pmatrix} x_1 \\ \phi_1 \end{pmatrix} = \begin{pmatrix} r_1 \\ r_2 \end{pmatrix} A(T_2)e^{i\omega T_0} + \text{c.c.}$$

$$(A.6)$$

where c.c. and $(r_1, r_2)^{\mathrm{T}}$ represent the complex conjugate of its preceding terms and a right eigenvector with respect to the critical eigenvalue. Substituting Eq. (A.6) into Eq. (A.5) yields

$$\mathbf{N}_2 = \mathbf{N}_{2,0} + \mathbf{N}_{2,2} + \text{c.c.},$$

$$(A.7)$$

where

$$\mathbf{N}_{2,0} = \begin{pmatrix} \psi \\ 1 \end{pmatrix} \frac{1}{\omega_0}\left(-i\omega r_2(1 - e^{-i\omega\tau_{1,0}})(v_c\overline{r_2} - \overline{r_1})e^{i\omega\tau_{1,0}}A(T_2)\overline{A}(T_2)\right),$$

$$\mathbf{N}_{2,2} = \begin{pmatrix} \psi \\ 1 \end{pmatrix} \frac{1}{\omega_0}\left(i\omega r_2(1 - e^{-i\omega\tau_{1,0}})(v_c r_2 - r_1)e^{-i\omega\tau_{1,0}}A^2(T_2)e^{2i\omega T_0}\right),$$

$$(A.8)$$

and $\overline{\bullet}$ is the complex conjugate of $\bullet$. By introducing

$$\mathbf{C}_2 = -4\omega^2 \mathbf{I} + 2i\omega \mathbf{C} + \mathbf{K} + (1 - e^{-i2\omega\tau_{1,0}})\mathbf{D},$$

$$(A.9)$$

34

one obtains the particular solution of Eq. (A.4) as follows

$$\mathbf{x}_2 = \begin{pmatrix} x_2 \\ \phi_2 \end{pmatrix} = \mathbf{K}^{-1}\mathbf{N}_{2,0} + \mathbf{C}_2^{-1}\mathbf{N}_{2,2} + \text{c.c..} \tag{A.10}$$

Then substituting Eqs (A.1), (A.2), (A.6) and (A.10) into Eq. (13), collecting the coefficients of ϵ^3 and eliminating the secular terms proportional to $e^{i\omega T_0}$ by Fredholm Alternative [38], one obtains the governing equation of $A(T_2)$ as follows

$$\frac{\partial A(T_2)}{\partial T_2} = \Lambda_1 A(T_2) + \Lambda_3 A(T_2)^2 \overline{A}(T_2), \tag{A.11}$$

where $\Lambda_1 = 0$ and the expression of Λ_3 is omitted for brevity. The criticality of the Hopf bifurcation is determined by the sign of Λ_3, where positive and negative values of Λ_3 indicate subcritical and supercritical Hopf bifurcations, respectively.

Acknowledgement

References

[1] Y. Liu, J. Páez Chávez, R. De Sa, S. Walker, Numerical and experimental studies of stickslip oscillations in drill-strings, Nonlinear Dynamics 90 (4) (2017) 2959–2978. `doi:10.1007/s11071-017-3855-9`.

[2] A. Ghasemloonia, D. Geoff Rideout, S. D. Butt, A review of drillstring vibration modeling and suppression methods, Journal of Petroleum Science and Engineering 131 (2015) 150–164. `doi:10.1016/j.petrol.2015.04.030`.

[3] S. Jardine, D. Malone, M. Sheppard, Putting a damper on drilling's bad
vibrations, Oilfield Review 6 (1) (1994) 15–20.

[4] B. Saldivar, S. Mondié, S. I. Niculescu, H. Mounier, I. Boussaada, A control
oriented guided tour in oilwell drilling vibration modeling, Annual Reviews
in Control 42 (2016) 100–113. `doi:10.1016/j.arcontrol.2016.09.002`.

[5] U. J. F. Aarsnes, O. M. Aamo, Linear stability analysis of self-excited
vibrations in drilling using an infinite dimensional model, Journal of Sound
and Vibration 360 (2016) 239–259. `doi:10.1016/j.jsv.2015.09.017`.

[6] D. Bresch-Pietri, M. Krstic, Output-feedback adaptive control of a wave
pde with boundary anti-damping, Automatica 50 (5) (2014) 1407–1415.
`doi:10.1016/j.automatica.2014.02.040`.

[7] X. Liu, N. Vlajic, X. Long, G. Meng, B. Balachandran, Nonlinear mo-
tions of a flexible rotor with a drill bit: stick-slip and delay effects, Non-
linear Dynamics 72 (1-2) (2013) 61–77, nonlinear Dyn. `doi:10.1007/
s11071-012-0690-x`.

[8] L. P. P. de Moraes, M. A. Savi, Drill-string vibration analysis considering an
axial-torsional-lateral nonsmooth model, Journal of Sound and Vibration
438 (2019) 220–237. `doi:10.1016/j.jsv.2018.08.054`.

[9] Y. Liu, Y. Ji, A. J. Dick, Numerical investigation of lateral and axial wave
propagation in drill-strings for stability monitoring, Journal of Vibration
and Acoustics 137 (4) (2015) 041014. `doi:10.1115/1.4029992`.

[10] M. Kapitaniak, V. Vaziri Hamaneh, J. Páez Chávez, K. Nandakumar,
M. Wiercigroch, Unveiling complexity of drillstring vibrations: Experi-
ments and modelling, International Journal of Mechanical Sciences 101-102
(2015) 324–337. `doi:10.1016/j.ijmecsci.2015.07.008`.

[11] M. Kapitaniak, V. Vaziri, J. Pez Chvez, M. Wiercigroch, Numerical study
of forward and backward whirling of drill-string, Journal of Computational
and Nonlinear Dynamics`doi:10.1115/1.4037318`.

36

[12] T. Richard, C. Germay, E. Detournay, A simplified model to explore the root cause of stickslip vibrations in drilling systems with drag bits, Journal of Sound and Vibration 305 (3) (2007) 432–456. `doi:10.1016/j.jsv.` 425 `2007.04.015`.

[13] B. Besselink, N. van de Wouw, H. Nijmeijer, A semi-analytical study of stick-slip oscillations in drilling systems, Journal of Computational and Nonlinear Dynamics 6 (2) (2010) 021006–021006–9. `doi:10.1115/1.` `4002386`.

430 [14] K. Nandakumar, M. Wiercigroch, Stability analysis of a state dependent delayed, coupled two dof model of drill-string vibration, Journal of Sound and Vibration 332 (10) (2013) 2575–2592. `doi:10.1016/j.jsv.2012.12.` `020`.

[15] S. K. Gupta, P. Wahi, Criticality of bifurcation in the tuned axialtorsional 435 rotary drilling model, Nonlinear Dynamics 91 (1) (2018) 113–130. `doi:` `10.1007/s11071-017-3859-5`.

[16] M. Wiercigroch, K. Nandakumar, L. Pei, M. Kapitaniak, V. Vaziri, State dependent delayed drill-string vibration: theory, experiments and new model, Procedia IUTAM 22 (2017) 39–50. `doi:10.1016/j.piutam.2017.` 440 `08.007`.

[17] J. Niu, Y. Ding, L. Zhu, H. Ding, Mechanics and multi-regenerative stability of variable pitch and variable helix milling tools considering runout, International Journal of Machine Tools and Manufacture 123 (Supplement C) (2017) 129–145. `doi:10.1016/j.ijmachtools.2017.08.006`.

445 [18] R. N. Arnold, The mechanism of tool vibration in the cutting of steel, Archive: Proceedings of The Institution of Mechanical Engineers 154 (1946) 261–284.

[19] S. A. Tobias, Machine tool vibration research, International Journal of Machine Tool Design and Research 1 (12) (1961) 1–14.

37

[20] Y. Yan, J. Xu, M. Wiercigroch, Estimation and improvement of cutting safety, Nonlinear Dynamicsdoi:10.1007/s11071-019-04980-0.

[21] X. Long, D. Meng, Y. Chai, Effects of spindle speed-dependent dynamic characteristics of ball bearing and multi-modes on the stability of milling processes, Meccanica 50 (12) (2015) 3119–3132. doi:10.1007/s11012-015-0183-3.

[22] Y. Yan, J. Xu, M. Wiercigroch, Stability and dynamics of parallel plunge grinding, The International Journal of Advanced Manufacturing Technology 99 (1) (2018) 881–895. doi:10.1007/s00170-018-2440-9.

[23] M. B. S. Marquez, I. Boussaada, H. Mounier, S.-l. Niculescu, Analysis and Control of Oilwell Drilling Vibrations A Time-Delay Systems Approach, Springer International Publishing, Switzerland, 2015.

[24] Y. Yan, J. Xu, M. Wiercigroch, Modelling of regenerative and frictional cutting dynamics, International Journal of Mechanical Sciences 156 (2019) 86–93. doi:10.1016/j.ijmecsci.2019.03.032.

[25] E. Detournay, T. Richard, M. Shepherd, Drilling response of drag bits: Theory and experiment, International Journal of Rock Mechanics and Mining Sciences 45 (8) (2008) 1347–1360. doi:10.1016/j.ijrmms.2008.01.010.

[26] S. K. Gupta, P. Wahi, Global axialtorsional dynamics during rotary drilling, Journal of Sound and Vibration 375 (2016) 332–352. doi:10.1016/j.jsv.2016.04.021.

[27] Y. Yan, J. Xu, M. Wiercigroch, Regenerative and frictional chatter in plunge grinding, Nonlinear Dynamics 86 (1) (2016) 283–307. doi:10.1007/s11071-016-2889-8.

[28] Y. Yan, J. Xu, M. Wiercigroch, Basins of attraction of the bistable region of time-delayed cutting dynamics, Physical Review E 96 (3) (2017) 032205. doi:10.1103/PhysRevE.96.032205.

[29] J. Xu, X. Sun, A multi-directional vibration isolator based on quasi-zero-stiffness structure and time-delayed active control, International Journal of Mechanical Sciences 100 (2015) 126–135. `doi:10.1016/j.ijmecsci.2015.06.015`.

[30] S. Zhang, J. Xu, K.-w. Chung, Desynchronization-based congestion suppression for a star-type internet system with arbitrary dimension, Neurocomputing 266 (2017) 42–55. `doi:10.1016/j.neucom.2017.05.023`.

[31] J. Ge, J. Xu, Z. Li, Zero-hopf bifurcation and multistability coexistence on a four-neuron network model with multiple delays, Nonlinear Dynamics 87 (4) (2017) 2357–2366. `doi:10.1007/s11071-016-3195-1`.

[32] Q. Xu, G. Stépán, Z. Wang, Delay-dependent stability analysis by using delay-independent integral evaluation, Automatica 70 (2016) 153–157. `doi:10.1016/j.automatica.2016.03.028`.

[33] B. Zhen, J. Xu, Z. Song, Lateral periodic vibrations of footbridges under crowd excitation, Nonlinear Dynamics 86 (3) (2016) 1701–1710. `doi:10.1007/s11071-016-2987-7`.

[34] S. K. Gupta, P. Wahi, Bifurcations in the axialtorsional state-dependent delay model of rotary drilling, International Journal of Non-Linear Mechanics 99 (2018) 13–30. `doi:10.1016/j.ijnonlinmec.2017.10.018`.

[35] T. G. Molnar, Z. Dombovari, T. Insperger, G. Stepan, On the analysis of the double hopf bifurcation in machining processes via centre manifold reduction, Proceedings of the Royal Society A: Mathematical, Physical and Engineering Science 473 (2017) 20170502. `doi:10.1098/rspa.2017.0502`.

[36] Z. Dombovari, G. Stepan, On the bistable zone of milling processes, Philosophical Transactions of the Royal Society A: Mathematical, Physical and Engineering Sciences 373 (2015) 1–17. `doi:10.1098/rsta.2014.0409`.

[37] X. Sun, J. Xu, F. Wang, S. Zhang, A novel isolation structure with flexible joints for impact and ultralow-frequency excitations, International

39

505 Journal of Mechanical Sciences 146-147 (2018) 366–376. `doi:10.1016/j.ijmecsci.2018.08.009`.

[38] A. H. Nayfeh, Order reduction of retarded nonlinear systems the method of multiple scales versus center-manifold reduction, Nonlinear Dynamics 51 (2008) 483500. `doi:10.1007/s11071-007-9237-y`.

510 [39] X. Sun, F. Wang, J. Xu, Dynamics and realization of a feedback-controlled nonlinear isolator with variable time delay, Journal of Vibration and Acoustics 141 (2) (2018) 021005. `doi:10.1115/1.4041369`.